Cancer Biol Med 2026. doi: 10.20892/j.issn.2095-3941.2025.0247

ORIGINAL ARTICLE

OPEN ACCESS

SPRED2 suppresses the stemness of hepatocellular carcinoma through the p53/miR-506-3p/KLF4 pathway

Tong Gao[1], Sachio Ito[2], Aye Moh-Moh-Aung[1], Tianyi Wang[1], Masayoshi Fujisawa[1], Toshiaki Ohara[1], Teizo Yoshimura[1], Akihiro Matsukawa[1]

[1]Department of Pathology and Experimental Medicine, Graduate School of Medicine, Dentistry and Pharmaceutical Sciences, Okayama University, Okayama 700-8558, Japan; [2]Department of Pathophysiology and Drug Discovery, Graduate School of Medicine, Dentistry and Pharmaceutical Sciences, Okayama University, Okayama 700-8558, Japan

ABSTRACT

Objective: We previously reported that endogenous Sprouty-related, EVH1 domain-containing protein 2 (SPRED2), an inhibitor of the Ras/Raf/ERK-MAPK pathway, controls hepatocellular carcinoma (HCC) cell stemness by downregulating the expression of pluripotency factors, such as Nanog, c-Myc, and KLF4, in an ERK-dependent fashion. However, the exact mechanisms by which SPRED2 regulates HCC cell stemness have not been established.

Methods: Three human HCC cell lines [HepG2 (parental and SPRED2-deficient), HLE, and Hep3B] were used. Cells were transfected to downregulate or overexpress proteins. Western blot and RT-qPCR were used to evaluate the level of protein and mRNA expression. Co-immunoprecipitation and ChIP-qPCR were used to examine protein-protein interactions and the activation of gene transcription. Clinical HCC tissues were also used to validate *in vitro* data.

Results: KLF4 was identified as the major pluripotency factor responsible for SPRED2-mediated downregulation of HCC cell stemness and KLF4 expression was regulated by miR-506-3p. SPRED2 formed a protein complex with the tumor suppressor (p53) and upregulated *miR-506* gene transcription by binding to the promoter region, resulting in subsequent downregulation of KLF4 mRNA expression. There was a negative correlation between KLF4 expression and miR-506-3p and a positive correlation between miR-506-3p expression and SPRED2 in human HCC samples, highlighting the relevance of the study findings.

Conclusions: The current study revealed a novel SPRED2/p53/miR-506-3p/KLF4 axis through which SPRED2 contributes to the suppression of HCC cell stemness and provides a potential new target to prevent HCC progression.

KEYWORDS SPRED2; p53; KLF4; miR-506-3p; stemness

Introduction

Liver cancer is the fifth most frequently diagnosed cancer and the second leading cause of cancer deaths worldwide. Hepatocellular carcinoma (HCC) accounts for 70–85% of cases among primary liver cancers with a 5-year recurrence rate as high as 70–80%[1]. Accumulating evidence suggests that cancer stem cells (CSCs) with a capacity for self-renewal and multipotency contribute to HCC initiation and progression. Although CSCs represent only a small proportion of the general population of cancer cells, CSCs contribute significantly to tumor relapse, metastasis, and chemoresistance[2]. CSC stemness is regulated by a complex interplay of networks, including transcriptional, post-transcriptional, and epigenetic regulation. In addition, signaling pathways create interwoven networks of signaling molecules and control CSCs[3]. It is critical to identify factors that control the intricate networks that regulate the stemness of CSCs to overcome HCC progression and chemoresistance.

Sprouty-related, EVH1 domain-containing protein 2 (SPRED2) is a member of the SPRED protein family. SPRED2 inhibits Ras-dependent extracellular signal-regulated kinase (ERK) signaling by suppressing Raf phosphorylation and activation[4]. SPRED2 expression is downregulated in advanced human cancers, such as prostate cancer[5], urothelial carcinoma[6], and HCC[7]. We and others have shown that SPRED2 overexpression decreases cancer cell motility and epithelial-mesenchymal transition (EMT)[8-11], apoptosis[8,12], and autophagy[13]. We also showed that SPRED2 knockout (KO) HCC cells have an increased ability to form spheres and colonies and express higher levels of stemness markers, such as Nanog, c-Myc, and KLF4[8]. The levels of Nanog, c-Myc, and KLF4 expression in HCC tissues were significantly higher

Correspondence to: Akihiro Matsukawa
E-mail: amatsu@md.okayama-u.ac.jp
Received May 19, 2025; accepted October 17, 2025;
published online January 20, 2026.
Available at www.cancerbiomed.org

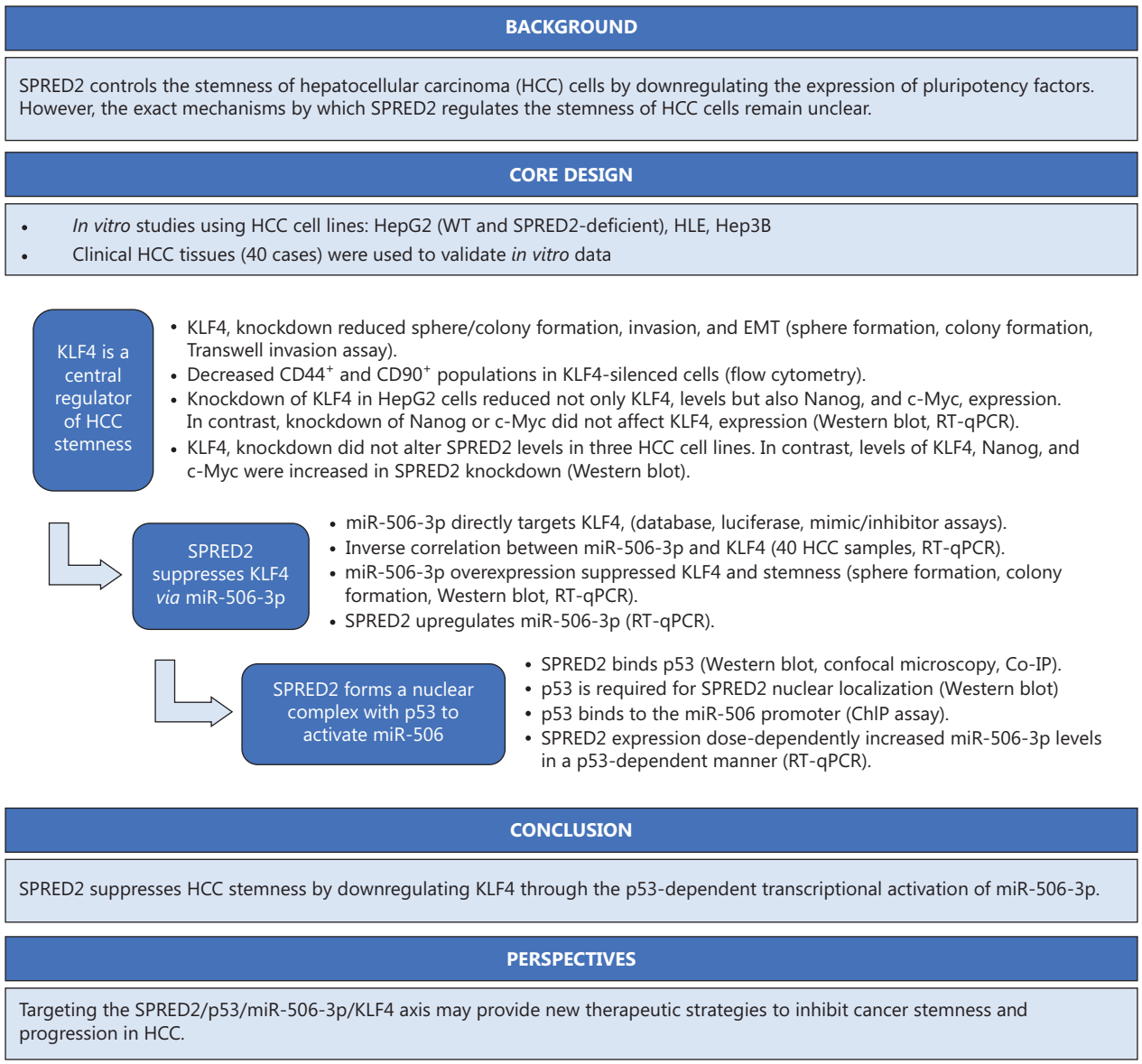

Study flowchart Three human HCC cell lines [HepG2 (parental and SPRED2-deficient), HLE, and Hep3B] were used. Cells were transfected to downregulate or overexpress proteins. Western blot and RT-qPCR were used to evaluate the level of protein and mRNA expression. Co-immunoprecipitation and ChIP-qPCR were used to examine protein–protein interactions and the activation of gene transcription. Clinical HCC tissues were also used to validate *in vitro* data. Therefore, the SPRED2/p53/miR-506-3p/KLF4 axis could be considered a target to prevent HCC progression through stemness regulation. ChIP, chromatin immunoprecipitation; Co-IP, co-immunoprecipitation; EMT, epithelial-mesenchymal transition; HCC, hepatocellular carcinoma; KLF4, Krüppel-like factor 4; miR, micro RNA; SPRED2, Sprouty-related, EVH1domain-containing protein 2; WT, wild-type.

than adjacent non-cancerous tissues. Interestingly, there was a significant negative correlation between SPRED2 and KLF4 mRNA expression[8]. Thus, endogenous SPRED2 has a critical role in suppressing cancer stemness in HCC cells. However, detailed mechanisms underlying SPRED2-mediated stemness suppression remain to be elucidated.

In the present study the molecular mechanisms leading to suppression of stemness by SPRED2 were elucidated. The study results showed that SPRED2 is a novel binding partner of the tumor suppressor (p53), enters the nucleus as the p53-SPRED2 complex, and upregulates *miR-506* gene transcription. Increased miR-506-3p targets KLF4 mRNA and reduces the KLF4 level, resulting in the subsequent downregulation of cancer cell stemness in HCC cells. Thus, the SPRED2/p53/miR-506-3p/KLF4 axis could be considered as a target to prevent HCC progression through stemness regulation.

Materials and methods

Cell culture

HepG2 and HLE cells (JCRB Cell Bank, Osaka, Japan) were cultured in Dulbecco's modified Eagle medium (Nacalai Tesque, Kyoto, Japan) supplemented with 10% fetal bovine serum (FBS) (Gibco, Carlsbad, CA, USA), 100 U/mL of penicillin, and 100 μg/mL of streptomycin (Sigma-Aldrich, St. Louis, MO, USA). Hep3B cells (DS Pharma Biomedical, Osaka, Japan) were cultured in Eagle's minimal essential medium (MEM; Sigma-Aldrich, St. Louis, MO, USA) (Sigma-Aldrich) supplemented with MEM non-essential amino acid solution, 10% FBS, and antibiotics. Cells were treated with the MEK/ERK1/2 inhibitor, PD98059 (20 μM; Thermo Fisher Scientific, Waltham, MA, USA), the STAT3 inhibitor, S3I-201 (20 μM; Abcam, Cambridge, UK), or vehicle (DMSO; FUJIFILM Wako Pure Chemical Corporation, Osaka, Japan) for 24 h in some experiments. All experiments were performed using mycoplasma-free cells.

Transfection

Cells (2×10^5 cells) were suspended in OPTI-MEM™ I reduced serum medium (Gibco; Thermo Fisher Scientific, Waltham, MA, USA) and seeded into 6-well plates. Transfection was performed using Lipofectamine 3000 (Life Technologies, Carlsbad, CA, USA) with reagents for loss- or gain-of-function experiments (**Table S1**) according to the manufacturer's protocol. Cells were then cultured for 48 h. The efficacy of each procedure was validated by real-time quantitative polymerase chain reaction (RT-qPCR) or Western blot.

Sphere formation and colony formation assay

Cells were dissociated into single cell suspensions when at approximately 80% confluence using 0.25% trypsin and 0.05% EDTA (Sigma-Aldrich, St. Louis, MO, USA). Cells were suspended in B-27 supplement (Thermo Fisher Scientific, Waltham, MA, USA), supplemented DMEM/F12 medium containing 20 ng/mL of epidermal growth factor (EGF) (Peprotech, Cranbury, NJ, USA) and 20 ng/mL of basic fibroblast growth factor (bFGF) (PeproTech, Rocky Hill, NJ, USA), seeded into 96-well ultra-low attachment plates (Corning, Lowell, MA, USA) at a density of 1000 cells per well, and incubated at 37°C. Fresh aliquots of EGF and bFGF were added every 2 d and cultured for a total of 14 days. The spheres were then dissociated, and cells (1×10^4 cells) were plated in a 6-well plate (BioLite 6-well multi-dish; Thermo Fisher Scientific, Waltham, MA, USA) and cultured for an additional 14 d to examine the self-renewal ability of the cells through secondary sphere formation. Images were captured using an inverted microscope (Olympus, Tokyo, Japan) at the indicated time points. Experiments were performed in triplicate.

Transwell invasion assay

Transwell chambers (Corning Incorporated, Corning, NY, USA) were used. Cells (2×10^5 cells) were seeded in the Matrigel-containing upper chambers and incubated for 24 h at 37°C. Cells that invaded to the lower surface of membranes were fixed with methanol and stained with crystal violet. Three low-power fields (magnification, ×20) were randomly selected from each membrane to count the number of migrated cells. Experiments were performed in triplicate.

Aldehyde dehydrogenase (ALDH) assay

ALDH activity was measured in cell lysates using the EnzyChrom™ ALDH Assay Kit (BioAssay Systems, Hayward, state, USA) according to the manufacturer's protocol. Absorbance was measured at 565 nm and enzyme activity was calculated based on a standard curve. The results were shown as relative ALDH activity normalized to the protein concentration. Four independent experiments were performed.

Human HCC xenograft model

Male Scid/beige mice (8 weeks of age) were purchased from The Jackson Laboratory Japan (Hamamatsu, Japan) and housed under specific pathogen-free conditions. HepG2 cells were transfected with control siRNA (si-Ctrl) or KLF4-specific siRNA (si-KLF4) (Dharmacon, Horizon Discovery, Lafayette, CO, USA) and cultured until confluent. The cells were then harvested and resuspended in culture medium without FBS or antibiotics. Five mice received subcutaneous injections of 5×10^6 viable si-Ctrl- and si-KLF4-transfected HepG2 cells (100 μL each) in the right and left dorsum, respectively. Tumor size was measured every 3 d after the tumor became palpable (day 7). Tumor volume was calculated using the following formula: volume = $(\text{width})^2 \times \text{length}/2$. The mice were sacrificed 28 d after implantation and the tumors were collected and photographed.

The experimental protocols used in this study were reviewed and approved by the Animal Care and Use Committee at Okayama University [Okayama, Japan (Approval No. OKU-2025640)]. All procedures were carried out in strict accordance with the relevant guidelines and regulations.

Cell isolation

CD44 and CD90 microbeads (Miltenyi Biotec, Bergisch Gladbach, Germany) were used to isolate $CD44^+$ and $CD90^+$ cells, respectively, from single cell suspensions of HCC cells. The purity and viability of the cells were > 95%.

Real-time quantitative PCR (RT-qPCR)

Total RNA was isolated from cultured cells using the High Pure RNA Isolation Kit (Roche, Mannheim, Germany). First-strand cDNA was synthesized from 2 μg of total RNA using a High-Capacity cDNA Reverse Transcription Kit (Thermo Fisher Scientific, Waltham, MA, USA). RT-qPCR was performed using a StepOnePlus™ Real-Time PCR System (Thermo Fisher Scientific, Waltham, MA, USA). The primers used in this study are listed in **Table S2**. The expression of each gene was normalized to GAPDH expression. miR-191-5p was used to validate miR-506-3p expression[14]. miR-191-5p was previously shown to be statistically superior to the reference RNAs, such as 5S rRNA, U6 snRNA, or total RNA, most frequently used in microRNA (miRNA) RT-qPCR experiments[15].

Western blot

Cells were lysed in lysis buffer (Cell Signaling Technology, Danvers, MA, USA). The protein concentration in lysates was measured using the BCA protein assay (Takara Bio, Shiga, Japan). Equal amounts of samples (15 μg) were fractionated by sodium dodecyl sulfate-polyacrylamide gel electrophoresis (SDS–PAGE; Thermo Fisher Scientific, Waltham, MA, USA) and proteins were transferred to PVDF membranes (Bio-Rad Laboratories, Hercules, CA, USA). The membranes were blocked, then incubated overnight with a primary antibody followed by a horseradish peroxidase-conjugated secondary antibody. Target proteins were visualized using ImmunoStar LD (Wako, Osaka, Japan) and the membranes were scanned using a C-DiGit Blot Scanner (LI-COR Biotechnology, Lincoln, NE, USA). The blot images were semi-quantified using Image Studio Digits software (LI-COR Biosciences, Lincoln, NE, USA). The antibodies used for Western blot are listed in **Table S3**.

Flow cytometry

Cells were incubated with Alexa Fluor 488-conjugated anti-human CD44 antibody and anti-human CD90 antibody (Biolegend, San Diego, CA, USA) to detect $CD44^+$ and $CD90^+$ cells, respectively. Cells were analyzed using a MACSQuant Analyzer (Miltenyi Biotec, Bergisch Gladbach, Germany) and data were analyzed using MACSQuantify software (Miltenyi Biotec, Bergisch Gladbach, Germany).

Dual-luciferase reporter assay

A double-stranded synthetic DNA with 60 base pairs containing a potential miR-506-3p targeting site in the 3′-UTR of the KLF4 gene (Thermo Fisher Scientific, Waltham, MA, USA) was cloned into the pmirGLO Dual-Luciferase miRNA Target Expression Vector (Promega, Madison, WI, USA) at the XbaI restriction enzyme site. A mutant 3′-UTR construct (Thermo Fisher Scientific, Waltham, MA, USA) was also generated by replacing the targeting site of the seed region with thymine (T) (Thermo Fisher Scientific). HepG2 cells were seeded into 24-well plates for 24 h until 60–70% confluence was reached, then transfected with 3 types of constructs and 30 picomol of miR-506-3p mimic using Lipofectamine™ RNAiMAX (Life Technologies, Thermo Fisher Scientific, Waltham, MA, USA). Each sample was cultured in duplicates for 48 h. The cell lysates were harvested to determine the firefly and Renilla luciferase activity using a Dual-Luciferase® Reporter Assay System (Promega Corporation, Madison, WI, USA) and luciferase activities were recorded using a GloMax® 96 Microplate Luminometer (Promega Corporation, Madison, WI, USA). The luminescence value was normalized by calculating the ratio of firefly luminescence-to-Renilla luminescence. Three independent experiments were performed.

Fluorescence immunostaining

Cells (1×10^4 cells) were seeded into the chambers of an 8-chamber Lab-Tek II Slide (Electron Microscopy Sciences, Hatfield, PA, USA) for cell staining, incubated at 37°C for 1 d, then fixed in acetone. HCC tissue sections (4-μm thick specimens) were deparaffinized, rehydrated, treated with 0.3% H_2O_2 in methanol, then subjected to heat-induced epitope retrieval in 1 mM ethylenediaminetetraacetic acid (EDTA) buffer (pH 8.0). The samples were incubated with the indicated primary antibody (**Table S3**) overnight at 4°C, followed by incubation with Alexa Fluor 568–conjugated goat anti-rabbit IgG and Alexa Fluor 647–conjugated goat anti-mouse IgG (Thermo Fisher Scientific, Waltham, MA, USA) for 30 min at room temperature, coverslipped with mounting medium containing DAPI, and visualized by confocal laser scanning microscopy (LSM780; Zeiss Microscopy, Jena, Germany). Co-localization of SPRED2 and p53 was assessed by calculating Pearson's correlation coefficient (r) using the Coloc2 plugin in ImageJ, as previously described[16]. Pearson's r values range from −1 and +1 with 0.0–0.3 considered low, 0.3–0.7 moderate, and 0.7–1.0 high degrees of co-localization.

Chromatin immunoprecipitation quantitative PCR (ChIP-qPCR)

ChIP analysis was performed according to the iDeal ChIP-qPCR Kit protocol (Diagenode, Denville, NJ, USA). HCC cells were cross-linked with 11% formaldehyde and lysed with cell lysis buffer. DNA was then sonicated to 200~500 bp using Bioruptor (Cosmo Bio Co., LTD, Tokyo, Japan). Lysates were incubated with rabbit anti-p53 mAb (catalog # 2527; Cell Signaling) or mouse anti-histone H3 mAb (catalog # 14269; Cell Signaling) with shaking at 4°C overnight. Normal rabbit IgG (catalog # 2729; Cell Signaling Technology,

Danvers, MA, USA) or normal mouse IgG (catalog # 5415; Cell Signaling Technology, Danvers, MA, USA) was used as a control (**Table S3**). DNA-protein-antibody complexes were then bound on Protein A beads (Invitrogen, Thermo Fisher Scientific, Waltham, MA, USA). After washing, the DNA-protein complexes were digested with Proteinase K (Diagenode, Liège, Belgium), followed by DNA purification using a DNA purification kit (Diagenode). qPCR was performed using primers amplifying the promoter region of the miR-506 gene, as follows: forward, 5′ CTTAGACTCTGCGTATGAGTC 3′; and reverse, 5′ GTCACCACAGTCATGCACTTG 3′. Data were calculated and expressed as % recovery = 2^(Ct_input − Ct_sample) × 100%.

Human tissue samples

An *a priori* power analysis was performed to determine the required sample size for a paired comparison between tumor and adjacent non-tumor tissues. The analysis indicated a minimum requirement of 33 paired samples, assuming a medium effect size (Cohen's $dz = 0.5$), a two-tailed significance level ($\alpha = 0.05$), and a statistical power (0.80). A total of 40 paired samples were included to account for potential unusable samples. This calculation corresponds to 40 subjects who provided tumor and adjacent matched non-tumor measurements. A total of 40 surgically resected HCC specimens (**Table S4**) were retrieved from the pathology records at Okayama University Hospital. The patients who received chemotherapy or radiotherapy before the resection were not included in this study. Hematoxylin and eosin (HE)-stained sections were reviewed by two pathologists in a blinded manner and the corresponding paraffin block was used for immunohistochemistry and RT-qPCR. RNA was isolated from the adjacent normal and cancerous areas of each sample. The level of the target gene expression was evaluated by RT-qPCR. RT-qPCR was performed on 1 sample from each case and on 40 independent human samples. Thus, there were 40 biological replicates and 1 technical replicate. Multiple RT-PCR tests were performed on some samples to ensure consistency of results and these measurements were considered precise. The study protocol was reviewed and approved by the Ethics Committee of Okayama University (1703-007). The study plan was posted on our website to allow patients or their families to opt out only cases from individuals who did not decline were enrolled in the study.

Analysis of database

Four miRNA databases [mirDIP (http://ophid.utoronto.ca/mirDIP/), DIANATOOLS (http://diana.imis.athena-innovation.gr/DianaTools/index.php), miRDB (http://mirdb.org), and Target Scan Human (http://www.targetscan.org/vert_72/)], a transcription factor-microRNA regulation database [Trans miR v2.0 database (http://www.cuilab.cn/transmir)], and a transcription factor binding profile [JASPAR (https://jaspar.elixir.no)] were used in the current study.

Statistical analysis

All statistical analyses were performed using SPSS statistics (version 25; IBM, Chicago, IL, USA) and GraphPad Prism 9 (GraphPad Software, San Diego, CA, USA). Levene's test was performed prior to group comparisons in IBM SPSS to assess homogeneity of variances. The assumption of equal variances was considered satisfied when the variances between groups were not significantly different ($P > 0.05$). Data distribution normality within each group was evaluated by the Shapiro–Wilk test in GraphPad Prism. All data in this study met the assumptions of equal variances and normality. A one-way ANOVA was performed in GraphPad Prism to assess group differences involving multiple groups. The overall ANOVA *P*-value was > 0.05, indicating that there were no statistically significant differences among the groups. In addition, a Brown–Forsythe test was used to assess homogeneity of variances. The Brown–Forsythe test yielded a *P*-value > 0.05, which supports the assumption of equal variances and validates the use of a standard ANOVA. The Bonferroni/Holm-Sidak/FDR correction method was used with the "Multiple *t* tests" module in GraphPad Prism for comparisons involving multiple genes of interest between control and experimental groups. This approach automatically adjusts *P*-values to account for multiple testing, thereby reducing the risk of false positives.

The statistical significance between the two groups with a normal distribution was analyzed with a parametric two-tailed unpaired *t*-test. A paired Student's *t*-test was used to analyze the differences between tumor and adjacent non-tumor tissues. Pearson's correlation was used to measure the degree of the relationship between two data. Data are expressed as the mean ± SEM. A *P*-value < 0.05 was considered statistically significant.

Results

KLF4 has an important role in regulating HCC stemness

We previously reported that *SPRED2* mRNA expression in cancer tissues was significantly lower than adjacent non-cancer tissues. In contrast, Nanog, c-Myc, and KLF4 expression in cancer tissues was significantly higher than adjacent non-cancer tissues. There was a significant negative correlation between SPRED2 and KLF4 mRNA expression but not between Nanog and c-Myc mRNA expression[8]. This finding suggested that KLF4 is the primary pluripotency factor influenced by SPRED2. KLF4 is one of the factors involved in the

induction of pluripotency in somatic cells and has been shown to be responsible for stem cell self-renewal, cancer initiation, progression, and metastasis in breast cancer[17]. KLF4 was knocked down in three HCC cell line cells by siRNA to clarify whether KLF4 has a major role in regulation of HCC stemness (**Figure S1A**). HepG2 cells were chosen as a model because HepG2 cells express a significant level of endogenous SPRED2 and are considered more suitable for the study than other cell lines, such as Hep3B and HLE cells, which express lower levels of SPRED2[8]. KLF4 knockdown HepG2 cells generated smaller spheres in a sphere-forming assay (**Figure 1A**), fewer colonies in a colony-forming assay (**Figure 1B**), and exhibited weaker invasion ability in a Transwell invasion assay (**Figure 1C**) compared to control HepG2 cells. EMT is often associated with acquisition of stemness properties in HCC cells[18]. KLF4 knockdown reversed cadherin switching, a hallmark of cells undergoing EMT[19], as evidenced by increased E-cadherin and decreased N-cadherin levels (**Figure 1D**). There was a trend towards decreased expression of the EMT-related transcription factor, Snail, in KLF4 knockdown cells (**Figure 1D**; $P = 0.0563$). ALDH activity, a functional marker for the stemness of cancer cells (including HCC cells)[20], was significantly reduced in KLF4 knockdown cells (**Figure 1E**). Similar results were obtained with KLF4 knockdown Hep3B and HLE cells (**Figure S1B-E**). In addition, KLF4 knockdown decreased the percentage of cells expressing $CD44^+$ (**Figure 1E**) or $CD90^+$ (**Figure 1F**), which are cell surface markers associated with CSCs[21,22]. HepG2 cells transfected with si-Ctrl or si-KLF4 (5×10^6 cells/site) were subcutaneously injected into SCID-beige mice to evaluate the effect of KLF4 knockdown on tumor growth *in vivo*. The tumor size was much smaller in the si-KLF4 group than the control group (**Figure 1H**). These results indicated that KLF4 is, at least in part, responsible for regulation of stemness in HCC cells.

We have previously shown that the expression of three pluripotency factors (Nanog, c-Myc and KLF4) are all increased in SPRED2-KO HepG2 cells[8]. Therefore, the role of KLF4 in SPRED2-mediated downregulation of stemness in HepG2 cells was investigated. Knockdown of KLF4 decreased the levels of KLF4 and Nanog and c-Myc in HepG2 cells (**Figure 2A**, left). In contrast, knockdown of Nanog (**Figure 2A**, middle) or c-Myc (**Figure 2A**, right) had no effects on KLF4 expression. These results indicated that KLF4 regulates Nanog and c-Myc expression in HepG2 cells. KLF4-mediated regulation of Nanog and c-Myc was also detected in other HCC cell lines [Hep3B (**Figure 2B**) and HLE (**Figure 2C**)].

In contrast, KLF4 does not appear to regulate SPRED2 expression in HCC cells because KLF4 knockdown did not alter SPRED2 expression in all three HCC cell lines (**Figure 2D, E**). In addition, increased Nanog and c-Myc expression in SPRED2-KO HepG2 cells was reduced to similar levels following KLF4 knockdown in WT HepG2 cells (**Figure 2F**). Finally, overexpressing SPRED2 in HepG2 cells reduced the expression of KLF4, c-Myc, and Nanog compared to the control (**Figure 2G**). Taken together, these results indicated that SPRED2 downregulates HCC cell stemness by targeting KLF4 expression.

KLF4 expression is regulated by miR-506-3p in HCC cells

Having identified that KLF4 is the critical factor regulating HCC cell stemness and that KLF4 expression is regulated by SPRED2, we asked how endogenous SPRED2 downregulates KLF4 expression in HCC cells. We focused on miRNAs because miRNAs are known to have a role in cancer development and progression[23]. Among miRNAs, the expression of miR-506-3p was previously shown to decrease in HCC tissues and the transfection of HCC cells with miR-506-3p significantly inhibited HCC cell proliferation *in vitro*[24,25]. Furthermore, miR-506-3p was shown to promote vascular smooth muscle cell proliferation and migration by targeting KLF4[26]. These findings led us to hypothesize that SPRED2 reduces KLF4 expression by increasing miR-506-3p expression.

To test this hypothesis, we searched for miR-506-3p targeting genes using four miRNA databases, including mirDIP, DIANATOOLS, miRDB, and Target Scan Human. KLF4 was 1 of the 553 genes common to all databases and identified as a candidate of the miR-506-3p target gene (**Figure S2**). When miR-506-3p expression was compared among the three HCC cell lines, miR-506-3p expression was significantly lower in Hep3B and HLE cells compared to HepG2 cells. Conversely, KLF4 expression was higher in Hep3B and HLE cells than HepG2 cells (**Figure 3A**). Next, HCC cells were transfected with control synthetic RNA and miR-506-3p-specific mimic or inhibitor (**Figure S3**). KLF4 mRNA and protein expression in HCC cells was decreased by the mimic, whereas KLF4 mRNA and protein expression in HCC cells was increased by the inhibitor (**Figure 3B**). Three luciferase reporter plasmids containing no additional sequence (control), wild-type (WT), or the mutated 3′-untranslated region (3′-UTR) sequence of KLF4 mRNA were prepared (**Figure 3C**) and HepG2 cells were transfected in combination with miR-506-3p mimic. miR-506-3p mimic decreased the luciferase activity by nearly 50% in cells transfected with the WT plasmid, whereas luciferase activity was not suppressed when the miR-506-3p targeting site was mutated (**Figure 3D**), further supporting our hypothesis.

The relationship between KLF4 mRNA and miR-506-3p expression in 40 clinical human HCC samples was analyzed to determine the relevance of the *in vitro* results (**Figure S4**). KLF4 mRNA expression was higher in tumor areas than adjacent non-tumor areas, whereas miR-506-3p expression was significantly lower in tumor areas than non-tumor areas (**Figure 3E**). There was a negative correlation between KLF4 mRNA and miR-506-3p expression in tumor areas

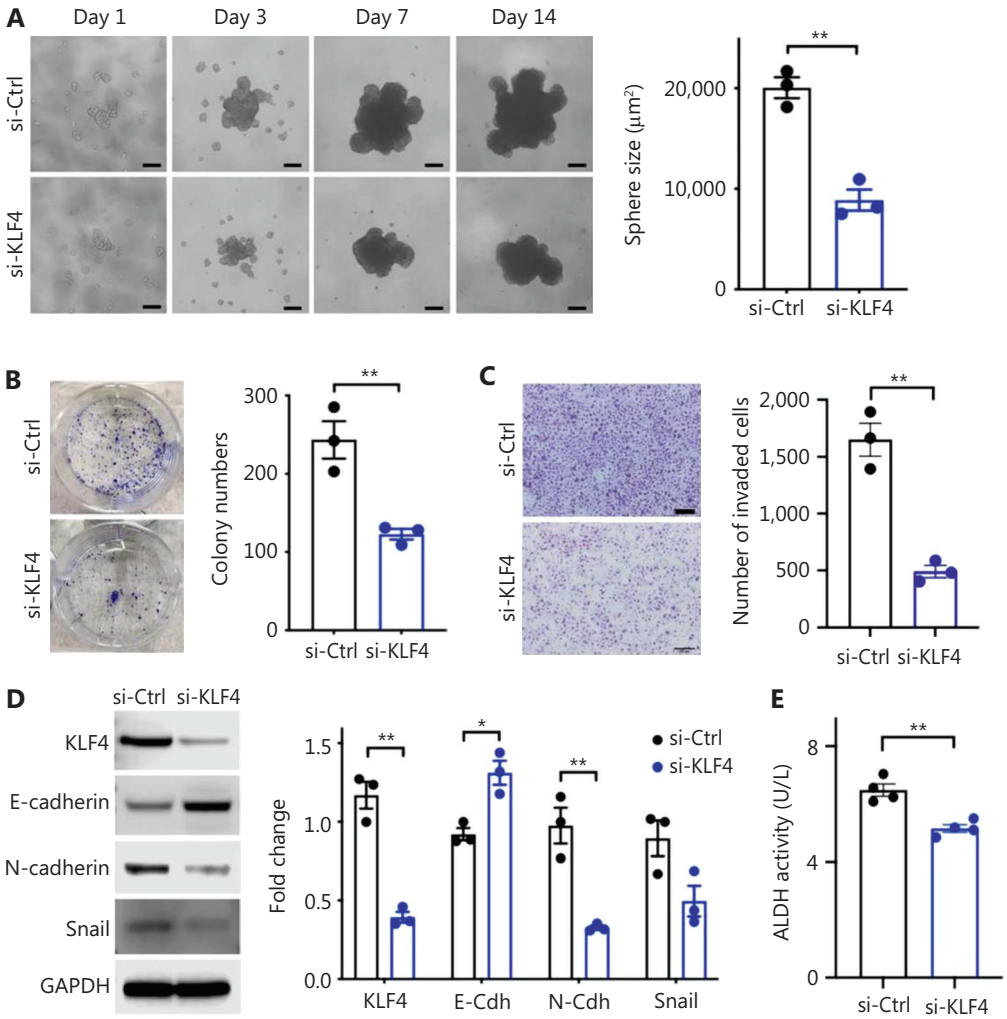

Figure 1 Continued

(**Figure 3F**). These results strongly suggested that miR-506-3p downregulates KLF4 expression in HCC cells by directly targeting the 3′-UTR of KLF4 mRNA.

miR-506-3p regulates KLF4 expression and HCC cell stemness

HepG2 cells were transfected with miR-506-3p mimic or inhibitor and the effects were evaluated using sphere- and colony-forming assays to obtain evidence indicating that miR-506-3p regulates HCC cell stemness. miR-506-3p mimic decreased the sphere- and colony-forming ability, while miR-506-3p inhibitor had an opposite effect (**Figure 4A, B**). Furthermore, miR-506-3p mimic decreased the levels of all three pluripotency factors (Nanog, c-Myc, and KLF4). In contrast, miR-506-3p inhibitor significantly increased KLF4 expression, while Nanog and c-Myc expression had an increasing trend but no significant differences (**Figure 4C**). Moreover, miR-506-3p mimic suppressed ALDH activity, whereas miR-506-3p inhibitor enhanced ALDH activity compared to the control group (**Figure 4D**).

Next, whether SPRED2 regulates the expression of miR-506-3p in HCC cells was determined. SPRED2 knockdown decreased miR-506-3p expression, whereas SPRED2 overexpression increased miR-506-3p expression (**Figure 4E**). In contrast, SPRED2 mRNA expression was unaffected by miR-506-3p mimic or inhibitor (**Figure 4F**). SPRED2 mRNA and miR-506 expression was analyzed in 40 pairs of HCC and adjacent non-cancer tissues by RT-qPCR (**Figure S4**). SPRED2 and miR-506-3p mRNA expression in cancer tissues was significantly lower than adjacent non-cancer tissues. Therefore, a positive correlation existed between SPRED2 and miR-506-3p expression in the tumor areas of HCC tissues (**Figure 4G**). These data supported the hypothesis that

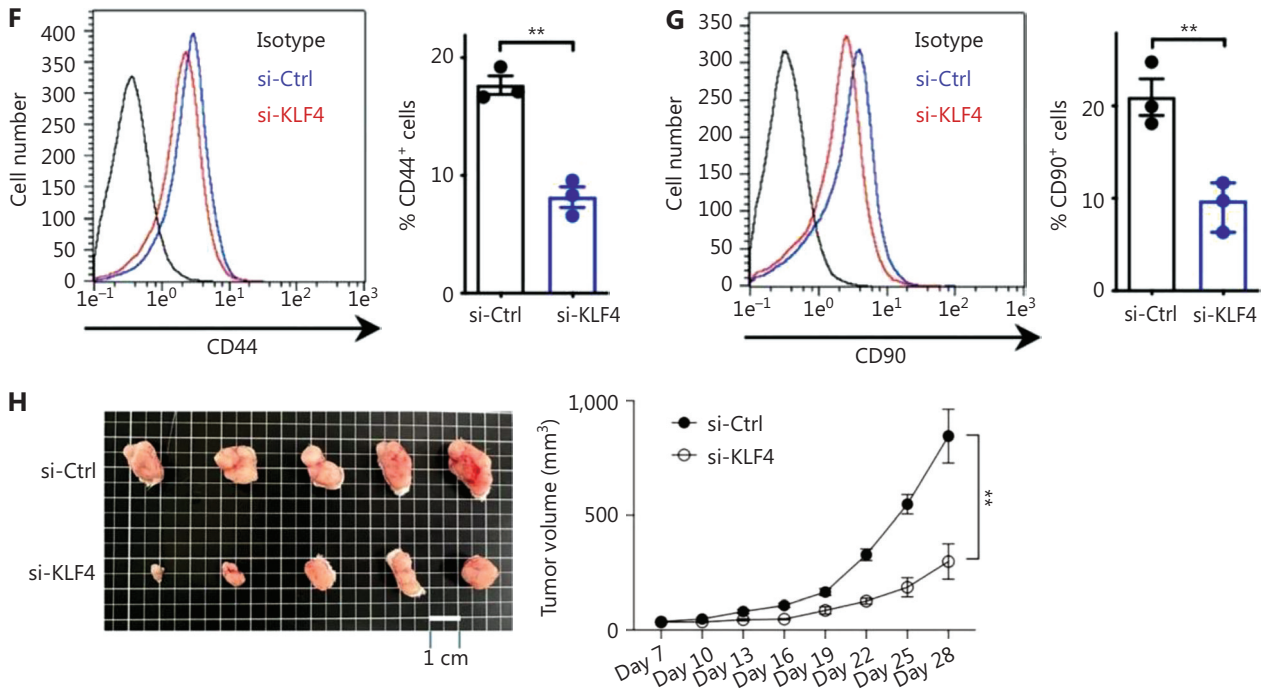

Figure 1 KLF4 regulates stemness in HepG2 cells. (A, B) HepG2 cells transfected with control siRNA (si-Ctrl) or KLF4-specific siRNA (si-KLF4) were cultured in 96-well ultra-low attachment plates for 14 days. (A) Left, representative photos are shown. Scale bars: 100 μm. Right, the sphere size was measured (n = 3 for each group). (B) Spherical colonies were dissociated and 1 × 10^4 cells were plated in 6-well plates and cultured for 14 days. Left, representative photos are shown. Right, the number of colonies was counted (n = 3 for each group). (C) Matrigel invasion assay was performed after transfection with control siRNA (si-Ctrl) or KLF4-specific siRNA (si-KLF4) in HepG2 cells. Left, representative photos are shown. Scale bars: 100 μm. Right, three low-power fields (100× magnification) were randomly selected from each membrane to count the number of migrated cells (n = 3 for each group). (D) The levels of each protein after transfection with control siRNA (si-Ctrl) or KLF4-specific siRNA (si-KLF4) in HepG2 cells were assessed by western blotting. Left, representative images are shown. Right, band densities were digitized and semi-quantified (n = 3 for each group). (E) HepG2 cells transfected with control siRNA (si-Ctrl) or KLF4-specific siRNA (si-KLF4) were extracted and the ALDH activities were measured (n = 4 for each group). (F, G) HepG2 cells were transfected with control siRNA (si-Ctrl) or KLF4-specific siRNA (si-KLF4). Left, cells were stained with Alexa Fluor 488-conjugated anti-human CD44 antibody (F) or anti-human CD90 antibody (G), and the percentage of positive cells was analyzed by flow cytometry. Right, the percentage of positive cells was evaluated (n = 3 for each group). (H) Five mice received subcutaneous injection of 5 × 10^6 viable si-Ctrl or si-KLF4 HepG2 cells (100 μL each) into the right and left dorsum, respectively. Tumor size was measured every 3 days for up to 28 days. Left, photographs of tumors resected on day 28. Right, tumor volume was calculated after the tumor became palpable. *P < 0.05, **P < 0.01, two-tailed unpaired t-test.

SPRED2 regulates miR-506-3p expression and subsequent KLF4 expression and HCC cell stemness.

SPRED2 binds to p53 and activates miR-506 gene transcription

SPRED2 is mainly located in the cytoplasm[27]. Therefore, it is unclear how SPRED2 regulates miR-506-3p expression. We speculated that SPRED2 may regulate miR-506-3p expression by binding to a transcription factor and translocation to the nucleus. Analysis of the Trans miR v2.0 database suggested that the tumor suppressor (p53) is a potential transcription factor activating miR-506 gene transcription (**Figure S3**). Whether SPRED2 was present in the nucleus of HepG2 cells was first examined by western blotting; SPRED2 was indeed present in the nucleus and cytoplasm (**Figure 5A**). SPRED2 was detected by immunofluorescence in the nucleus (**Figure 5B**) and co-localized with p53 in HepG2 cells (**Figure 5C**, upper) and clinical HCC tissues (**Figure 5C**, lower). Pearson r values were calculated (HepG2 cells, 0.5312; and HCC tissues, 0.2032), which indicated a moderate and low degree of co-localization of SPRED2 and p53, respectively. Co-immunoprecipitation (Co-IP) was performed to investigate the potential binding between p53 and SPRED2 in HepG2 cells (WT p53) and HLE cells (mutant p53). SPRED2 and p53 were co-immunoprecipitated by anti-p53 or anti-SPRED2 antibody (**Figure 5D**), strongly suggesting the ability of SPRED2 to bind p53. The hypothesis that p53 supports SPRED2 nuclear translocation

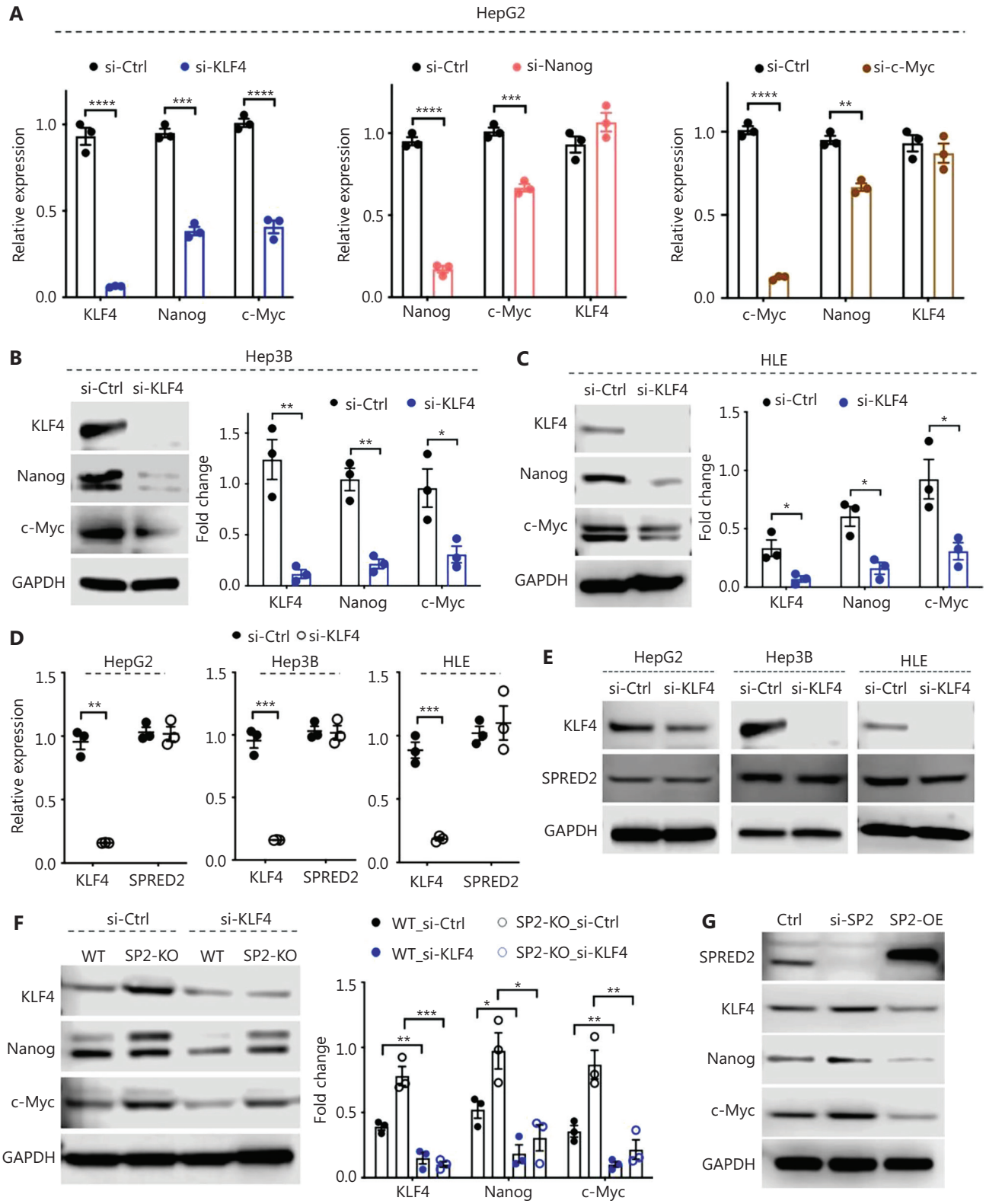

Figure 2 KLF4 has an important role in HCC stemness regulation. (A) HepG2 cells transfected with control siRNA (si-Ctrl) or KLF4/Nanog/c-Myc specific siRNA (si-KLF4/Nanog/c-Myc) were cultured in 6-well plates for 14 days. mRNA expression of KLF4, Nanog, and c-Myc were examined by RT-qPCR (n = 3 for each group). (B, C) Hep3B cells and HLE cells transfected with control siRNA (si-Ctrl) or KLF4-specific siRNA

(si-KLF4) were cultured in 6-well plates for 48 h. The level of each protein in Hep3B (B) and HLE cells (C) was assessed by western blotting. Left, representative images are shown. Right, band densities were digitized and semi-quantified (n = 3 for each group). (D, E) HepG2/Hep3B/HLE cells transfected with control siRNA (si-Ctrl) or KLF4-specific siRNA (si-KLF4) were cultured in 6-well plates for 48 h. (D) KLF4 and SPRED2 mRNA expression was examined by RT-qPCR (n = 3 for each group). (E) Production of each protein was assessed by western blotting. Representative images are shown. (F) Wild-type HepG2 (WT) and SPRED2-KO HepG2 cells (SP2-KO) transfected with control siRNA (si-Ctrl) or KLF4-specific siRNA (si-KLF4) were cultured in 6-well plates for 48 h. The level of each protein was assessed by western blotting. Left, representative images are shown. Right, band densities were digitized and semi-quantified (n = 3 for each group). (G) Cell lysates were prepared from control (Ctrl), SPRED2 knockdown (si-SP2), and SPRED2-overexpression (SP2-OE) cells and the presence of each protein was evaluated by western blotting. Representative data are shown. *P < 0.05, **P < 0.01, ***P < 0.001, ****P < 0.0001, two-tailed unpaired t-test.

by knocking down p53 (**Figure S5**) in HepG2 and HLE cells was tested next. Nuclear SPRED2 expression was decreased in p53-knockdown HepG2 and HLE cells compared to controls (**Figure 5E, F**). In contrast, nuclear SPRED2 expression was increased when p53 was overexpressed (**Figure S5**) in p53-deficient Hep3B cells[28] (**Figure 5G**).

The 5′-promoter region of the miR-506 gene was analyzed and a sequence with potential p53 binding ability was identified (**Figure 6A**). Significant enrichment of the miR-506 DNA promoter region sequence was detected by ChIP-qPCR using anti-p53 antibody compared to control IgG, indicating p53 binding to the promoter region of the miR-506 gene in both cell lines (**Figure 6B**). SPRED2 KO HepG2 cells were transfected by increasing doses of SPRED2-expression plasmid to confirm the role of SPRED2 and p53 in miR-506 gene transcription. SPRED2 increased miR-506-3p expression in a dose-dependent fashion (**Figure 6C**). Knockdown or overexpression of SPRED2 had no effect on miR-506-3p expression in Hep3B cells with absence of p53 and presence of SPRED2 (**Figure 6D**). However, miR-506-3p expression was increased when cells were transfected with p53-expression plasmid (**Figures S6 and 6E**). miR-506-3p expression was further increased compared to p53 overexpression alone when both SPRED2 and p53 were overexpressed (**Figure S6**), although not statistically significant (**Figure 6E**; P = 0.098).

These results strongly suggest that SPRED2 downregulates HCC cell stemness *via* enhanced miR-506 gene transcription by interacting with p53 and decreasing KLF4 expression.

Role of ERK and STAT3 in SPRED2-mediated miR-506-3p expression in HCC cells

SPRED2 inhibits ERK activation by binding to RAF and/or RSK2[4,29]. SPRED2 is also shown to inhibit STAT3 activation by interacting with DYRK1A[30]. STAT3 activation occurs during various aspects of carcinogenesis, including regulation of CSCs properties[31]. We recently showed that SPRED2 downregulated HCC cell stemness in an ERK-dependent manner. Furthermore, SPRED2 deletion increased STAT3 phosphorylation, whereas SPRED2 overexpression decreased[8]. The possibility that the ERK and the STAT3 pathways have a role in stemness *via* miR-506-3p expression in HCC cells was examined. S3I-201 (STAT3 inhibitor) significantly decreased the sphere size (**Figure 7A**) and downregulated KLF4, Nanog, and c-Myc expression was confirmed using HepG2 cells (**Figure 7B**). The role of ERK and STAT3 signaling in miR-506-3p expression was determined. PD98059 (ERK inhibitor) and S3I-201 increased miR-506-3p expression in HepG2 cells, as shown in **Figure 7C**. ERK activation, as evidenced by increased ERK phosphorylation, was not altered by S3I-201 and STAT3 activation, as evidenced by increased STAT3 phosphorylation, was not affected by PD98059 (**Figure 7D**), indicating that ERK and STAT3 independently suppresses miR-506-3p. This finding suggests that ERK and STAT3 inhibition by SPRED2 increases miR-506-3p expression and inhibits HCC cell stemness.

Discussion

The role of SPRED2 in cancer has attracted attention. We previously showed that endogenous SPRED2 inhibits not only proliferation, migration and invasion capacity, but also EMT and HCC cell stemness by downregulating the expression of pluripotency factors, such as Nanog, c-Myc, and KLF4. Among the pluripotency factors, only KLF4 had a negative correlation with *SPRED2* mRNA expression in human HCC tissues[8]. KLF4, one of the Yamanaka factors[32], has a strong oncogenic role in mammary tumorigenesis, probably by maintaining stem cell-like features[17]. In the present study the mechanisms by which SPRED2 mediates the downregulation of stemness in HCC cells were characterized. KLF4 was first identified as a critical pluripotency factor regulating HCC cell stemness. Interestingly, SPRED2 forms a protein complex with p53 that binds to a DNA sequence located upstream of the *miR-506* gene and increases gene transcription. miR-506-3p, a product of miR-506, downregulates KLF4 expression. Thus, we demonstrated a novel mechanism by which SPRED2 downregulates HCC cell stemness.

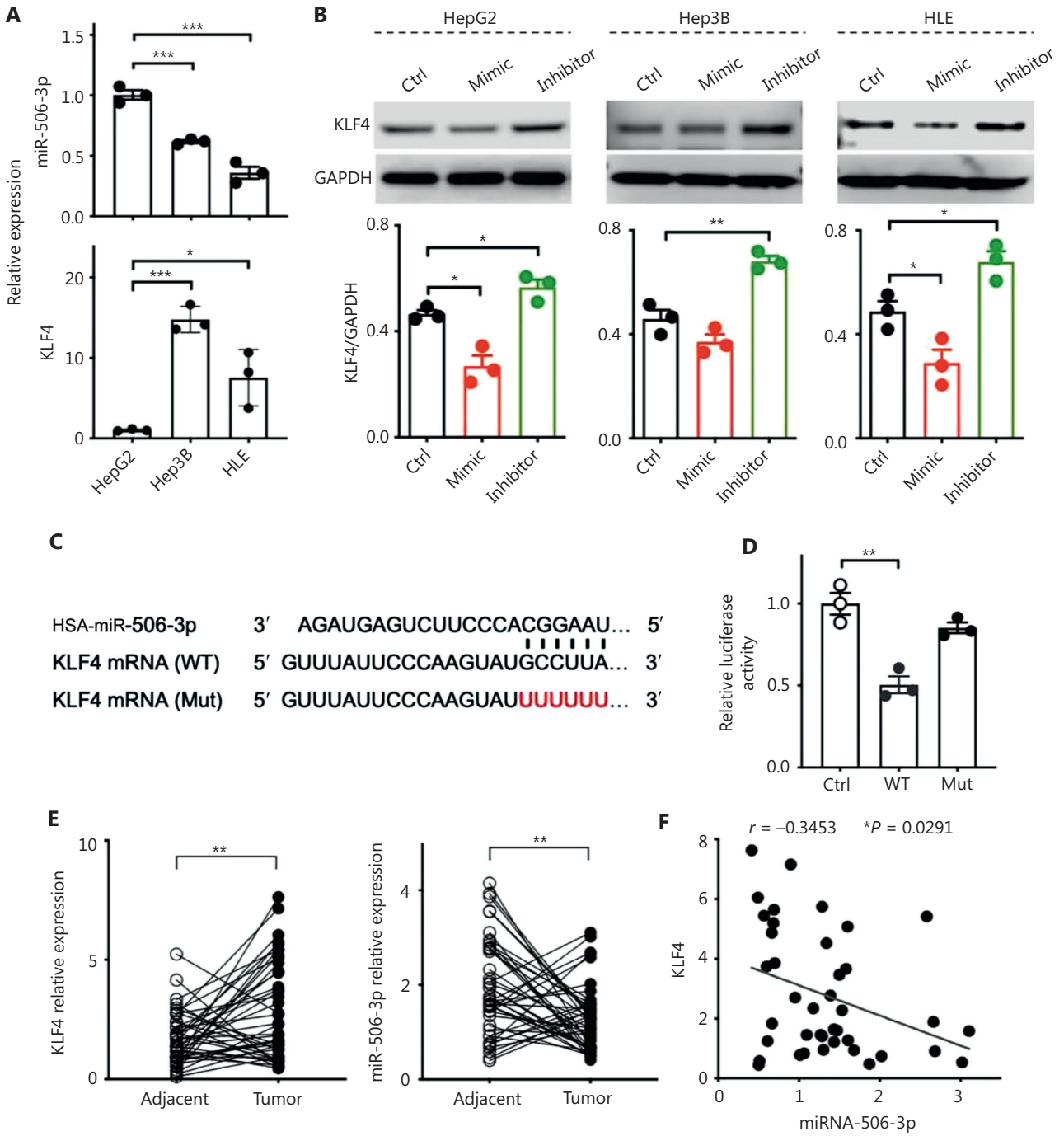

Figure 3 Expression of KLF4 is regulated by miR-506-3p in HCC cells. (A) Expression of miR-506-3p and KLF4 in HepG2, Hep3B, and HLE cells was examined by RT-qPCR (n = 3 for each group.). (B) miR-506-3p mimic or inhibitor was transfected into HepG2/Hep3B/HLE cells and the protein level of KLF4 was assessed by western blotting. Top, representative images are shown. Bottom, band densities were digitized and semi-quantified (n = 3 for each group). (C) The sequences of a potential miR-506-3p targeting site in the 3′-UTR of KLF4 mRNA, miR-506-3p, and mutant (red) are presented. (D) Luciferase activities after transfection with empty vector or constructs containing WT or a mutant KLF4 mRNA 3-UTR sequence were evaluated (n = 3 for each group). (E) Expression of miR-506-3p and KLF4 in 40 clinical samples was measured by RT-qPCR. (F) The relationship between miR-506-3p and KLF4 expression was analyzed. *P < 0.05, **P < 0.01, ***P < 0.001, two-tailed unpaired t-test.

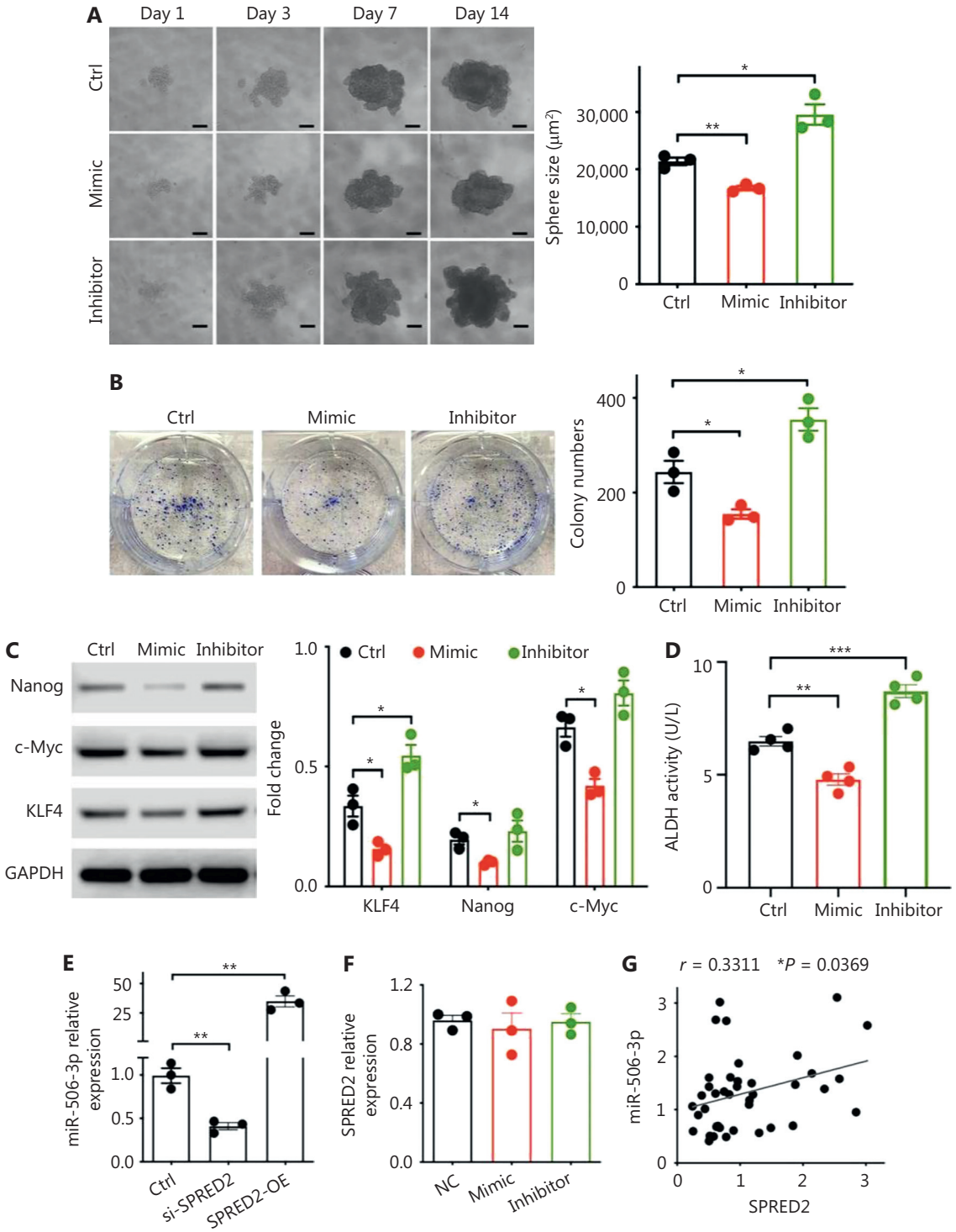

Figure 4 miR-506-3p regulates the expression of KLF4 and stemness in HCC cells. (A, B) HepG2 cells transfected with miR-506-3p mimic or inhibitor were cultured in 96-well ultra-low attachment plates for 14 days. (A) Left, representative photos are shown. Scale bars: 100 μm. Right, the sphere size was measured (n = 3 for each group). (B) Spherical colonies were dissociated and dispersed cells were plated in 6-well plates and cultured for 14 days. Left, representative photos are shown. Right, the number of colonies was counted (n = 3 for each group). (C, D) miR-506-3p mimic or inhibitor was transfected into HepG2 cells. (C) The level of each protein was assessed by western blotting. Left, representative images are shown. Right, band densities were digitized and semi-quantified (n = 3 for each group). (D) Cells were extracted and the ALDH

activities were measured (n = 4 for each group). (E) Expression of miR-506-3p in HepG2 cells transfected with control siRNA (si-Ctrl), SPRED2-specific siRNA (si-SPRED2), or SPRED2 overexpression plasmid (SPRED2-OE) was evaluated by RT-qPCR (n = 3 for each group). (F) HepG2 cells were transfected with miR-506-3p mimic or inhibitor and the SPRED2 mRNA level was measured by RT-qPCR (n = 3 for each group). (G) Expression of miR-506-3p and SPRED2 in 40 clinical samples was measured by RT-qPCR. The relationship between miR-506-3p and SPRED2 expression was analyzed. *P < 0.05, **P < 0.01, ***P < 0.001, two-tailed unpaired t-test.

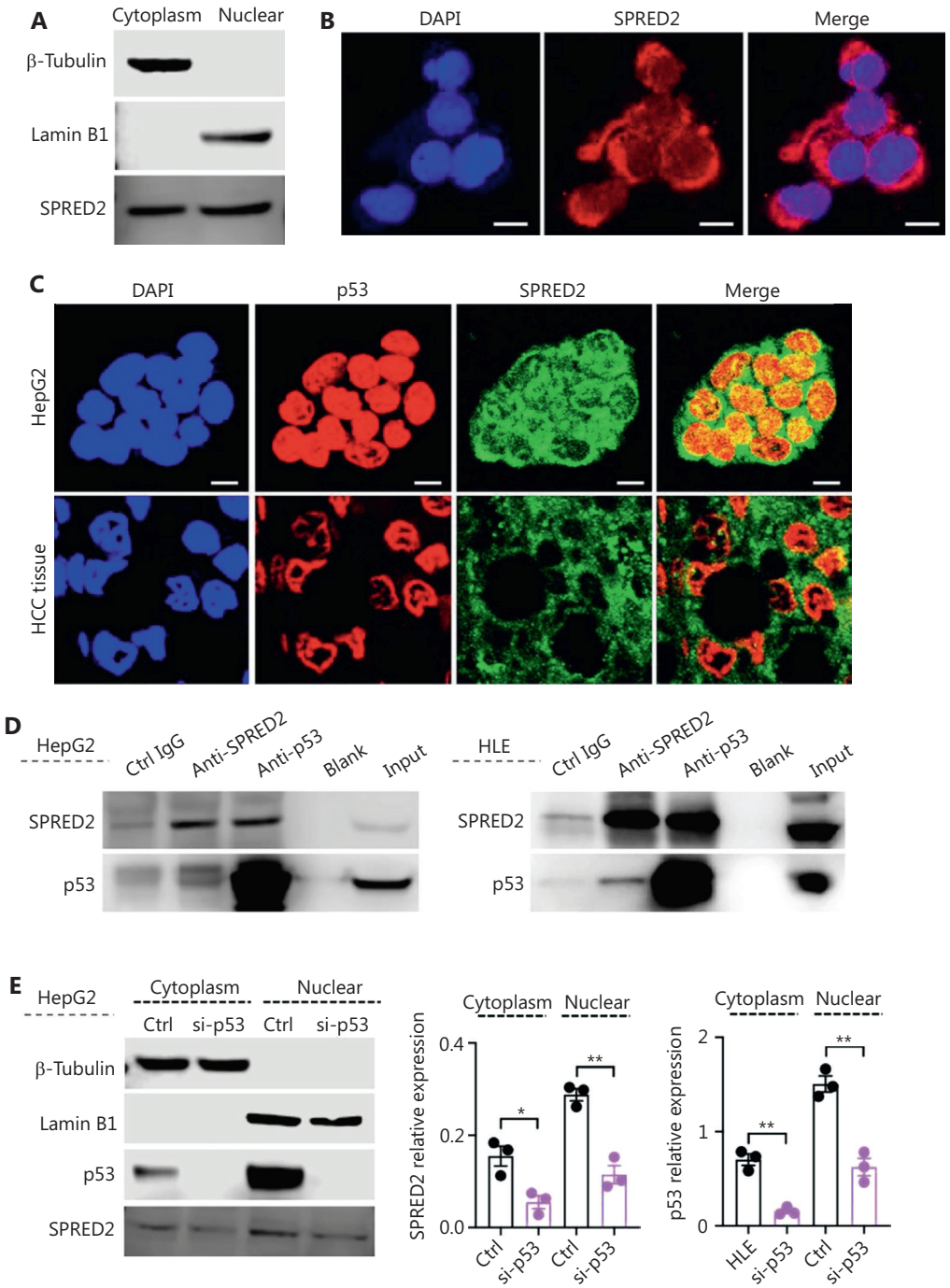

Figure 5 Continued

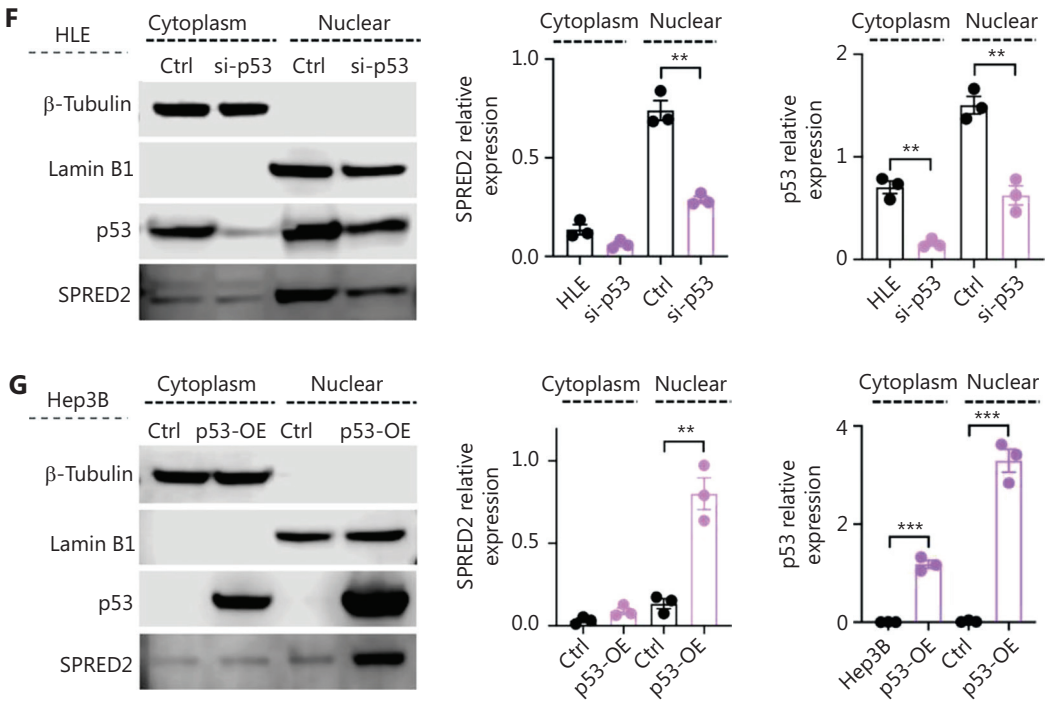

Figure 5 p53 supports nuclear translocation of SPRED2. (A) Cell lysates were prepared from the cytoplasm and nucleus of HepG2 cells and the presence of each protein was assessed by western blotting. β-Tubulin and lamin B1 were used as a cytoplasmic and nuclear protein marker, respectively. Representative images are shown. (B) HepG2 cells were seeded in Lab-Tek II slides, fixed in acetone, and stained with anti-SPRED2 antibody. Representative photos are shown. Scale bars: 10 μm. (C) Co-localization of SPRED2 and p53 in HepG2 cells (top) and clinical HCC samples (bottom) was examined by immunofluorescence using a confocal microscope. Representative photos are shown. Scale bars: 10 μm. (D) Cell lysates (1 mg) from HepG2 and HLE cells were incubated with anti-SPRED2 and anti-p53 antibodies. The immunoprecipitated proteins were separated by SDS-PAGE and the presence of each protein was analyzed by western blotting using anti-p53 and anti-SPRED2 antibodies, respectively. Representative images are shown. (E, F) HepG2 (E) and HLE cells (F) were transfected with control siRNA (si-Ctrl) or p53-specific siRNA (si-p53). Cytoplasmic and nuclear proteins were obtained from the cell lysates. The presence of each protein was determined by western blotting. β-Tubulin and lamin B1 were used as a cytoplasmic and nuclear protein marker, respectively. Left, representative images are shown. Right, band densities were digitized and semi-quantified using the appropriate controls (cytoplasm; β-tubulin: nuclear; lamin B1) (n = 3 for each group). (G) Hep3B cells were transfected with control (Ctrl) or p53 overexpression plasmid (p53-OE). Cytoplasmic and nuclear proteins were obtained from cell lysates. The presence of each protein was determined by western blotting. β-Tubulin and lamin B1 were used as a cytoplasmic and nuclear protein marker, respectively. Left, representative images are shown. Right, band densities were digitized and semi-quantified using the appropriate controls (cytoplasm; β-tubulin: nuclear; lamin B1) (n = 3 for each group). $^{**}P < 0.01$, $^{***}P < 0.001$, $^{****}P < 0.0001$, two-tailed unpaired t-test.

miRNAs are a class of small non-coding single-stranded RNAs, approximately 23 nucleotides in length, that regulate gene expression. miRNAs bind to the 3′-UTRs of the target mRNAs, resulting in mRNA degradation or translational repression[33]. Alterations in miRNA expression are involved in the initiation and progression of human cancers, including HCC. Profiling miRNA expression patterns in human tumors has identified signatures associated with diagnosis, staging, progression, prognosis, and response to treatment[23]. Among miRNAs, miR-506 is known to suppress tumorigenesis of HCC cells by targeting the 3′-UTR of YAP mRNA[34], Rho-associated protein kinase 1 (ROCK1)[35], and IL-8 mRNA[36]. The expression of miR-506-3p, a product of its precursor (miR-506), is decreased in several cancers and has been implicated in cancer progression[37,38] and EMT[39-42]. A set of 19 miR-506-3p target genes that function as strong modulators in neuroblastoma cell lines have been identified[43]. Herein we identified a novel miR-506-3p target site in the 3′-UTR of KLF4 mRNA and demonstrated that miR-506-3p suppresses cancer stemness by downregulating KLF4 mRNA expression. miR-506-3p expression was decreased in SPRED2 KO cells and increased upon SPRED2 overexpression in HCC cells. There was a positive correlation between SPRED2 and miR-506-3p expression in human HCC tissues. These results indicated that

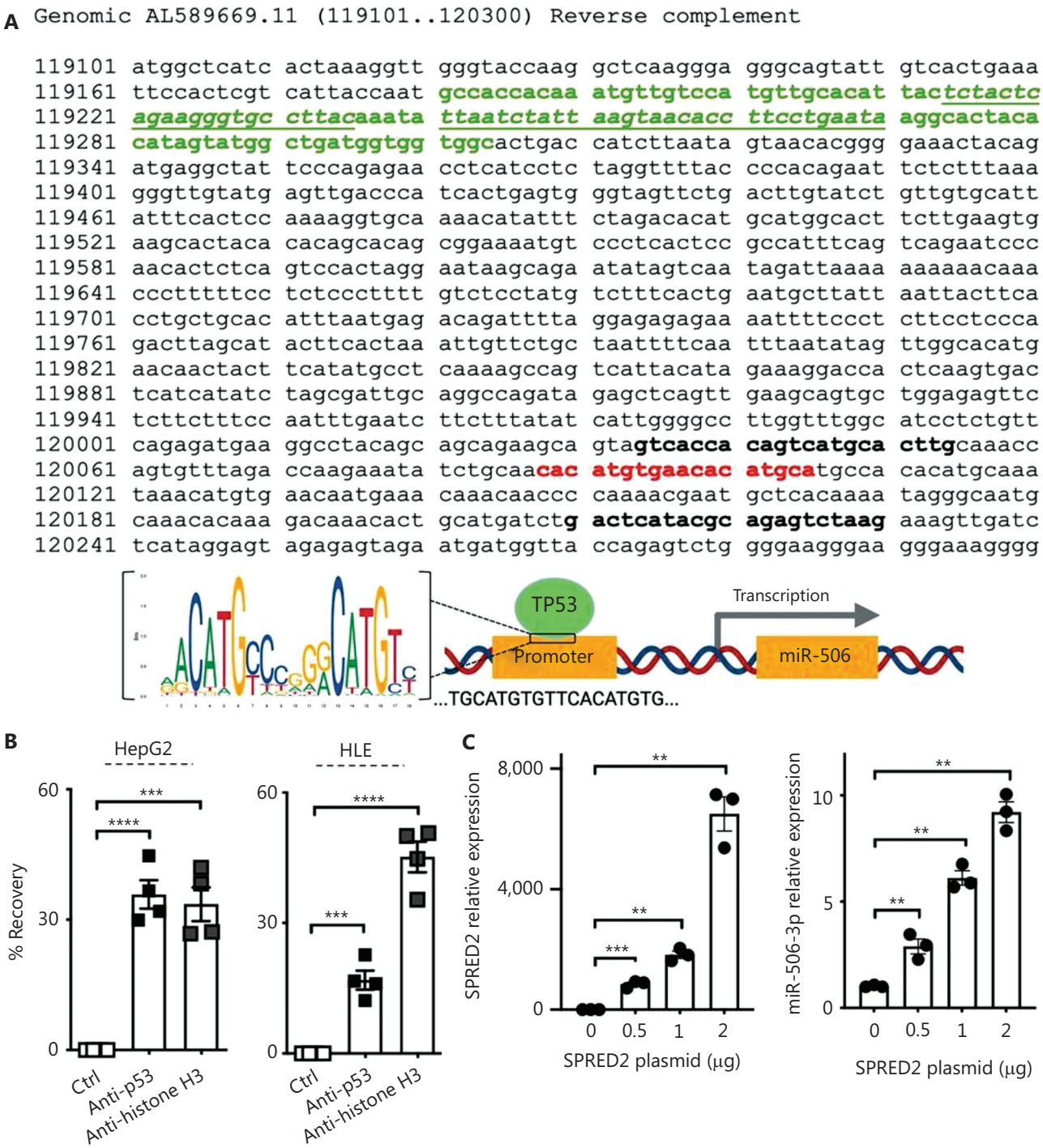

Figure 6 Continued

SPRED2 inhibits HCC cell stemness *via* miR-506-3p, which targets KLF4 mRNA.

p53, coded by the *TP53* gene, functions as a transcription factor that regulates cell proliferation, senescence, DNA repair, and cell death[44,45]. p53-deleted pancreatic epithelial cells display stemness features, such as increased sphere formation and increased expression of CSC markers[46]. p53 is a multidomain protein consisting of five main regions: the transactivation domain (TAD); proline-rich domain; DNA binding domain; tetramerization domain; and a regulatory domain.

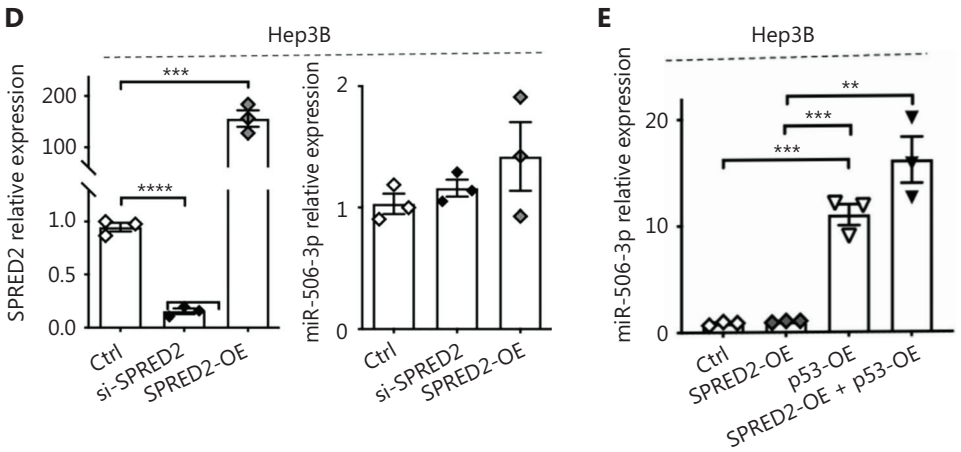

Figure 6 SPRED2/p53 complex binds to the promoter region of miR-506 gene. (A) Top, the nucleotide sequence of the miR-506 gene (complementary strand) is shown. Green: The miR-506 gene sequence. miR-506-5p and 3p sequences are underlined. Red: a potential p53 binding site in the 5′-upstream of the miR-506 gene. Bold letters: Primer sequences used for qPCR. Bottom, a p53 consensus binding site from the JASPAR database is shown. (B) HepG2a and HLE cells were cross-linked, lysed, sonicated, and the cell lysates were incubated with anti-p53 mAb or anti-histone H3 mAb. DNA-protein-antibody complexes were purified and qPCR was performed using primers for promoter region of the miR-506 gene. Data were calculated and expressed as % recovery = 2^(Ct_input − Ct_sample) × 100% (n = 4 for each group). (C) SPRED2-knockout HepG2 cells were transfected with 0.5, 1, or 2 μg of SPRED2 expression plasmid and the expression of SPRED2 (left) and miR-506-3p (right) was evaluated by RT-qPCR (n = 3 for each group). (D) Hep3B cells were transfected with SPRED2-specific siRNA (si-SPRED2) or SPRED2 overexpression plasmid (SPRED2-OE) and the expression of SPRED2 (left) and miR-506-3p (right) was evaluated by RT-qPCR (n = 3 for each group). (E) Hep3B cells were transfected with SPRED2 overexpression plasmid (SPRED2-OE) and p53 overexpression plasmid (p53-OE), and the expression of miR-506-3p was evaluated by RT-qPCR (n = 3 for each group). **P < 0.01, ***P < 0.001, ****P < 0.00001, two-tailed unpaired t-test.

The TAD allows p53 to bind several cofactors that contribute to p53 function in a context-dependent fashion[47,48]. We have shown for the first time that p53 forms a complex with SPRED2. SPRED2 was detected in the cytoplasm and nucleus in p53-present HepG2 and HLE cells but the nuclear SPRED2 level decreased after p53 knockdown. Overexpression of p53 increased nuclear SPRED2 expression in p53-deficient Hep3B, suggesting that a part of cytoplasmic SPRED2 translocates to the nucleus with p53. In addition, binding of SPRED2/p53 protein complex to the promoter region of the miR-506 gene was detected. These data strongly suggest that binding of SPRED2 enables p53 to activate *miR-506* gene transcription more efficiently. Further studies are needed to identify the binding domain of SPRED2 that is used to form a complex with p53 and to determine whether other proteins involved in gene transcription are included in the protein complex.

Accumulating evidence suggests that dysfunction of signaling pathways, including Janus-activated kinase/signal transducer and activator of transcription (JAK/STAT), Hedgehog, Wnt, Notch, phosphatidylinositol 3-kinase/phosphatase and tensin homolog (PI3K/PTEN), and nuclear factor-κB (NF-κB), supports unregulated self-renewal and differentiation of CSCs[49,50]. Many of these pathways are mediated by an interwoven network of signaling mediators that feedback on each of the pathways and promoting crosstalk between pathways. Aberrant activation of the JAK/STAT pathway has been shown in stem-like cells isolated from breast, prostate, blood, and glial tumors, and the activated form of STAT3 has been shown to be the most significantly upregulated JAK/STAT signaling protein in breast CSC-like cells[51]. The MAPK/ERK pathway also has an important role in regulating the self-renewal and differentiation of embryonic stem cells[52]. SPRED2 has been shown to inhibit the MAPK/ERK pathway by binding to RAF and/or RSK2[4,29] and the STAT3 pathway by binding to DYRK1A[30]. Inhibition of both signaling pathways can reduce KLF4 expression[30,53] and suppress stemness in SPRED2-expressing HCC cells. The interaction of these pathways is based on the previous findings and the present results are shown in **Figure 8**. SPRED2 binds to RAF and/or RSK2 and inhibits the ERK signaling pathway under normal conditions (left panel)[4,29]. SPRED2 also binds to DYRK1A and inhibits the STAT3 signaling pathway[30]. As a result, the inhibitory effect on miR-506-3p is negated, resulting in increased expression of miR-506. SPRED2 also forms a protein complex with p53 and directly promotes miR-506-3p expression. Thus, SPRED2 coordinates all three pathways (ERK, STAT3, and p53)

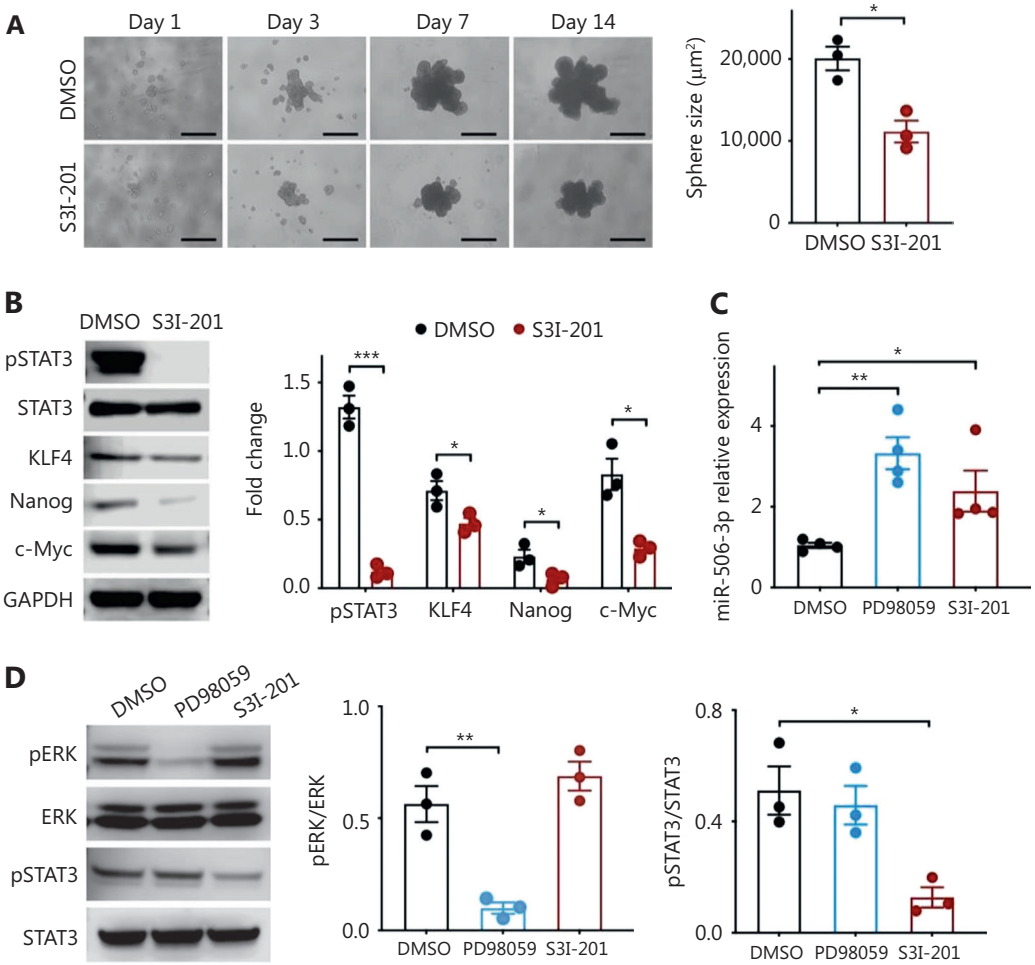

Figure 7 The role of ERK and STAT3 in SPRED2-mediated increased miR-506-3p expression and decreased HCC cell stemness. (A) HepG2 cells were cultured with 20 μM S3I-201 or vehicle (DMSO) in 96-well ultra-low attachment plates for 14 days. Left, representative photos are shown. Scale bars: 100 μm. Right, the sphere size was measured (n = 3 for each group). (B, C) HepG2 cells were cultured with 20 μM S3I-201 or vehicle (DMSO) for 24 h. (B) The levels of each protein in the cell lysates were evaluated by western blotting. Left, representative images are shown. Right, band densities were digitized and semi-quantified (n = 3 for each group). (C) miR-506-3p mRNA expression was evaluated by RT-qPCR (n = 3 for each group). (D) HepG2 cells were treated with 20 μM PD98059, 20 μM S3I-201, or vehicle (DMSO) for 24 h. Cell lysates were prepared and the level of each protein was evaluated by western blotting. Left, representative images are shown. Right, band densities were digitized and semi-quantified (n = 3 for each group). *P < 0.05, **P < 0.01, ***P < 0.001, two-tailed unpaired t-test.

to increase miR-506-3p expression, thereby reducing KLF4 expression and HCC cell stemness. The ERK and STAT3 pathways are no longer inhibited and the formation of SPRED2/p53 protein complex decreases when HCC cells lose the expression of SPRED2, leading to decreased miR-506-3p expression. This effect results in increased KLF4 expression and promotion of HCC stemness. It remains unknown whether ERK or STAT3 has a role in forming SPRED2/p53 complex or binding to the miR-506 gene promoter. More detailed studies are needed to clarify the interplay between the three pathways in regulation of KLF4 expression and subsequent cell stemness.

Conclusions

In summary, we have identified a novel action of SPRED2 in the regulation of HCC cell stemness. This action does not appear to require its inhibitory effects on the MAPK/ERK or STAT3 pathways. Molecules targeting signaling pathways have become a new direction for the treatment of HCC[54]. The identification of the SPRED2/p53/miR-506-3p/KLF4 axis may provide novel therapeutic strategies to prevent HCC progression.

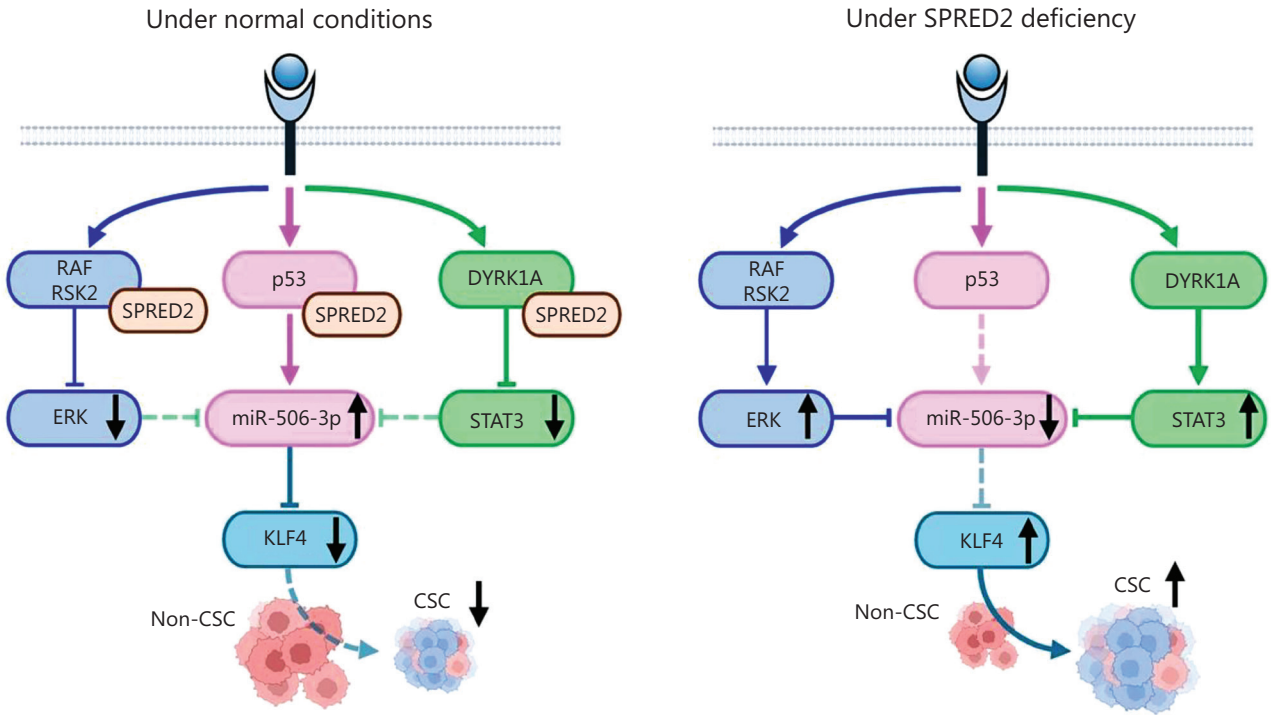

Figure 8 Schematic diagram indicating the mechanisms by which SPRED2 regulates the stemness of HCC cells. miR-506-3p downregulates KLF4 expression. Left panel: Under normal conditions, SPRED2 binds to RAF and/or RSK2 and inhibits the ERK signaling pathway. SPRED2 also binds to DYRK1A and inhibits the STAT3 signaling pathway. As a result, the inhibitory effect on miR-506-3p is negated, resulting in increased expression of miR-506. SPRED2 also forms a protein complex with p53 and directly promotes miR-506-3p expression. Thus, SPRED2 coordinates all three pathways (ERK, STAT3, and p53) to increase miR-506-3p expression, thereby reducing KLF4 expression and cell stemness in HCC cells. Right panel: When HCC cells lose the expression of SPRED2, the ERK and STAT3 pathways are no longer inhibited and the formation of SPRED2/p53 protein complex decreases, leading to decreased miR-506-3p expression. This results in increased KLF4 expression and promotion of HCC stemness.

Acknowledgments

We thank Hiroyuki Watanabe for his excellent technical assistance.

Grant support

This work was supported in part by Japan Society for the Promotion of Science (Grant Nos. 25293095, 90264283, and 22K19562).

Conflict of interest statement

No potential conflicts of interest are disclosed.

Author contributions

Conceived and designed the analysis: Tong Gao, Akihiro Matsukawa.

Collected the data: Tong Gao, Sachio Ito, Aye Moh-Moh-Aung, Tianyi Wang.

Contributed data or analysis tools: Masayoshi Fujisawa, Toshiaki Ohara.

Performed the analysis: Tong Gao, Teizo Yoshimura.

Wrote the paper: Tong Gao, Teizo Yoshimura, Akihiro Matsukawa.

Data availability statement

The data that support the findings of this study are available from the corresponding author upon reasonable request.

References

1. Nevola R, Ruocco R, Criscuolo L, Villani A, Alfano M, Beccia D, et al. Predictors of early and late hepatocellular carcinoma recurrence. World J Gastroenterol. 2023; 29: 1243-60.
2. Lee TK, Guan XY, Ma S. Cancer stem cells in hepatocellular carcinoma – from origin to clinical implications. Nat Rev Gastroenterol Hepatol. 2022; 19: 26-44.

3. Zeng Z, Fu M, Hu Y, Wei Y, Wei X, Luo M. Regulation and signaling pathways in cancer stem cells: implications for targeted therapy for cancer. Mol Cancer. 2023; 22: 172.
4. Wakioka T, Sasaki A, Kato R, Shouda T, Matsumoto A, Miyoshi K, et al. Spred is a Sprouty-related suppressor of Ras signalling. Nature. 2001; 412: 647-51.
5. Kachroo N, Valencia T, Warren AY, Gnanapragasam VJ. Evidence for downregulation of the negative regulator SPRED2 in clinical prostate cancer. Br J Cancer. 2013; 108: 597-601.
6. Oda S, Fujisawa M, Chunning L, Ito T, Yamaguchi T, Yoshimura T, et al. Expression of Spred2 in the urothelial tumorigenesis of the urinary bladder. PLoS One. 2021; 16: e0254289.
7. Yoshida T, Hisamoto T, Akiba J, Koga H, Nakamura K, Tokunaga Y, et al. Spreds, inhibitors of the Ras/ERK signal transduction, are dysregulated in human hepatocellular carcinoma and linked to the malignant phenotype of tumors. Oncogene. 2006; 25: 6056-66.
8. Gao T, Yang X, Fujisawa M, Ohara T, Wang T, Tomonobu N, et al. SPRED2: a novel regulator of epithelial-mesenchymal transition and stemness in hepatocellular carcinoma cells. Int J Mol Sci. 2023; 24: 4996.
9. Ma XN, Liu XY, Yang YF, Xiao FJ, Li QF, Yan J, et al. Regulation of human hepatocellular carcinoma cells by Spred2 and correlative studies on its mechanism. Biochem Biophys Res Commun. 2011; 410: 803-8.
10. Villar V, Kocić J, Santibanez JF. Spred2 inhibits TGF-beta1-induced urokinase type plasminogen activator expression, cell motility and epithelial mesenchymal transition. Int J Cancer. 2010; 127: 77-85.
11. Wang H, Liu S, Kong F, Xiao F, Li Y, Wang H, et al. Spred2 inhibits epithelial-mesenchymal transition of colorectal cancer cells by impairing ERK signaling. Oncol Rep. 2020; 44: 174-84.
12. Liu XY, Yang YF, Wu CT, Xiao FJ, Zhang QW, Ma XN, et al. Spred2 is involved in imatinib-induced cytotoxicity in chronic myeloid leukemia cells. Biochem Biophys Res Commun. 2010; 393: 637-42.
13. Wang T, Gao T, Fujisawa M, Ohara T, Sakaguchi M, Yoshimura T, et al. SPRED2 is a novel regulator of autophagy in hepatocellular carcinoma cells and normal hepatocytes. Int J Mol Sci. 2024; 25: 6269.
14. Grenda A, Nicoś M, Szczyrek M, Krawczyk P, Kucharczyk T, Jarosz B, et al. MicroRNAs aid the assessment of programmed death ligand 1 expression in patients with non-small cell lung cancer. Oncol Lett. 2019; 17: 5193-200.
15. Peltier HJ, Latham GJ. Normalization of microRNA expression levels in quantitative RT-PCR assays: identification of suitable reference RNA targets in normal and cancerous human solid tissues. RNA. 2008; 14: 844-52.
16. Shakhov AS, Kovaleva PA, Churkina AS, Kireev II, Alieva IB. Colocalization analysis of cytoplasmic actin isoforms distribution in endothelial cells. Biomedicines. 2022; 10: 3194.
17. Yu F, Li J, Chen H, Fu J, Ray S, Huang S, et al. Kruppel-like factor 4 (KLF4) is required for maintenance of breast cancer stem cells and for cell migration and invasion. Oncogene. 2011; 30: 2161-72.
18. Malfettone A, Soukupova J, Bertran E, Crosas-Molist E, Lastra R, Fernando J, et al. Transforming growth factor-β-induced plasticity causes a migratory stemness phenotype in hepatocellular carcinoma. Cancer Lett. 2017; 392: 39-50.
19. Giannelli G, Koudelkova P, Dituri F, Mikulits W. Role of epithelial to mesenchymal transition in hepatocellular carcinoma. J Hepatol. 2016; 65: 798-808.
20. Ma S, Chan KW, Lee TK, Tang KH, Wo JY, Zheng BJ, et al. Aldehyde dehydrogenase discriminates the CD133 liver cancer stem cell populations. Mol Cancer Res. 2008; 6: 1146-53.
21. Ji J, Wang XW. Clinical implications of cancer stem cell biology in hepatocellular carcinoma. Semin Oncol. 2012; 39: 461-72.
22. Yang ZF, Ho DW, Ng MN, Lau CK, Yu WC, Ngai P, et al. Significance of CD90+ cancer stem cells in human liver cancer. Cancer Cell. 2008; 13: 153-66.
23. Hussen BM, Hidayat HJ, Salihi A, Sabir DK, Taheri M, Ghafouri-Fard S. MicroRNA: a signature for cancer progression. Biomed Pharmacother. 2021; 138: 111528.
24. Xu H, Luo M, Xiang H, Liao W, Huang H, Wu Y, et al. miR-506-3p can inhibit cell proliferation and is a diagnostic and prognostic marker of liver cancer. Am J Transl Res. 2021; 13: 11531-9.
25. Yoshida K, Yokoi A, Yamamoto Y, Kajiyama H. ChrXq27.3 miRNA cluster functions in cancer development. J Exp Clin Cancer Res. 2021; 40: 112.
26. Dong H, Jiang G, Zhang J, Kang Y. MiR-506-3p promotes the proliferation and migration of vascular smooth muscle cells via targeting KLF4. Pathobiology. 2021; 88: 277-88.
27. Engelhardt CM, Bundschu K, Messerschmitt M, Renné T, Walter U, Reinhard M, et al. Expression and subcellular localization of Spred proteins in mouse and human tissues. Histochem Cell Biol. 2004; 122: 527-38.
28. Bressac B, Galvin KM, Liang TJ, Isselbacher KJ, Wands JR, Ozturk M. Abnormal structure and expression of p53 gene in human hepatocellular carcinoma. Proc Natl Acad Sci U S A. 1990; 87: 1973-7.
29. Lopez J, Bonsor DA, Sale MJ, Urisman A, Mehalko JL, Cabanski-Dunning M, et al. The ribosomal S6 kinase 2 (RSK2)-SPRED2 complex regulates the phosphorylation of RSK substrates and MAPK signaling. J Biol Chem. 2023; 299: 104789.
30. Li D, Jackson RA, Yusoff P, Guy GR. Direct association of Sprouty-related protein with an EVH1 domain (SPRED) 1 or SPRED2 with DYRK1A modifies substrate/kinase interactions. J Biol Chem. 2010; 285: 35374-85.
31. Wei S, Li J, Tang M, Zhang K, Gao X, Fang L, et al. STAT3 and p63 in the regulation of cancer stemness. Front Genet. 2022; 13: 909251.
32. Takahashi K, Tanabe K, Ohnuki M, Narita M, Ichisaka T, Tomoda K, et al. Induction of pluripotent stem cells from adult human fibroblasts by defined factors. Cell. 2007; 131: 861-72.
33. Shang R, Lee S, Senavirathne G, Lai EC. microRNAs in action: biogenesis, function and regulation. Nat Rev Genet. 2023; 24: 816-33.
34. Wang Y, Cui M, Sun BD, Liu FB, Zhang XD, Ye LH. MiR-506 suppresses proliferation of hepatoma cells through targeting YAP mRNA 3′UTR. Acta Pharmacol Sin. 2014; 35: 1207-14.

35. Deng Q, Xie L, Li H. MiR-506 suppresses cell proliferation and tumor growth by targeting Rho-associated protein kinase 1 in hepatocellular carcinoma. Biochem Biophys Res Commun. 2015; 467: 921-7.
36. Wang Z, Si M, Yang N, Zhang H, Fu Y, Yan K, et al. MicroRNA-506 suppresses invasiveness and metastasis of human hepatocellular carcinoma cells by targeting *IL8*. Am J Cancer Res. 2018; 8: 1586-94.
37. Huang B, Liu C, Wu Q, Zhang J, Min Q, Sheng T, et al. Long non-coding RNA NEAT1 facilitates pancreatic cancer progression through negative modulation of miR-506-3p. Biochem Biophys Res Commun. 2017; 482: 828-34.
38. Wang Y, Lei X, Gao C, Xue Y, Li X, Wang H, et al. MiR-506-3p suppresses the proliferation of ovarian cancer cells by negatively regulating the expression of MTMR6. J Biosci. 2019; 44: 126.
39. Haque I, Kawsar HI, Motes H, Sharma M, Banerjee S, Banerjee SK, et al. Downregulation of miR-506-3p facilitates EGFR-TKI resistance through induction of Sonic Hedgehog signaling in non-small-cell lung cancer cell lines. Int J Mol Sci. 2020; 21: 9307.
40. Liu Y, Yan W, Zhou D, Jin G, Cheng X. Long non-coding RNA HOXA11-AS accelerates cell proliferation and epithelial-mesenchymal transition in hepatocellular carcinoma by modulating the miR-506-3p/Slug axis. Int J Mol Med. 2020; 46: 1805-15.
41. Sun Y, Wu J, Dong X, Zhang J, Meng C, Liu G. MicroRNA-506-3p increases the response to PARP inhibitors and cisplatin by targeting EZH2/β-catenin in serous ovarian cancers. Transl Oncol. 2021; 14: 100987.
42. Wang D, Bao F, Teng Y, Li Q, Li J. MicroRNA-506-3p initiates mesenchymal-to-epithelial transition and suppresses autophagy in osteosarcoma cells by directly targeting SPHK1. Biosci Biotechnol Biochem. 2019; 83: 836-44.
43. Cardus DF, Smith MT, Vernaza A, Smith JL, Del Buono B, Parajuli A, et al. Systematic analysis of miR-506-3p target genes identified key mediators of its differentiation-inducing function. Genes (Basel). 2024; 15: 1268.
44. Hernández Borrero LJ, El-Deiry WS. Tumor suppressor p53: Biology, signaling pathways, and therapeutic targeting. Biochim Biophys Acta Rev Cancer. 2021; 1876: 188556.
45. Wang H, Guo M, Wei H, Chen Y. Targeting p53 pathways: mechanisms, structures, and advances in therapy. Signal Transduct Target Ther. 2023; 8: 92.
46. Pinho AV, Rooman I, Real FX. p53-dependent regulation of growth, epithelial-mesenchymal transition and stemness in normal pancreatic epithelial cells. Cell Cycle. 2011; 10: 1312-21.
47. Raj N, Attardi LD. The transactivation domains of the p53 protein. Cold Spring Harb Perspect Med. 2017; 7: a026047.
48. Sullivan KD, Galbraith MD, Andrysik Z, Espinosa JM. Mechanisms of transcriptional regulation by p53. Cell Death Differ. 2018; 25: 133-43.
49. Chen K, Huang YH, Chen JL. Understanding and targeting cancer stem cells: therapeutic implications and challenges. Acta Pharmacol Sin. 2013; 34: 732-40.
50. Matsui WH. Cancer stem cell signaling pathways. Medicine (Baltimore). 2016; 95: S8-19.
51. Zhou J, Wulfkuhle J, Zhang H, Gu P, Yang Y, Deng J, et al. Activation of the PTEN/mTOR/STAT3 pathway in breast cancer stem-like cells is required for viability and maintenance. Proc Natl Acad Sci U S A. 2007; 104: 16158-63.
52. Ma X, Chen H, Chen L. A dual role of Erk signaling in embryonic stem cells. Exp Hematol. 2016; 44: 151-6.
53. Rauluseviciute I, Riudavets-Puig R, Blanc-Mathieu R, Castro-Mondragon JA, Ferenc K, Kumar V, et al. JASPAR 2024: 20th anniversary of the open-access database of transcription factor binding profiles. Nucleic Acids Res. 2024; 52: D174-82.
54. Luo X, He X, Zhang X, Zhao X, Zhang Y, Shi Y, et al. Hepatocellular carcinoma: signaling pathways, targeted therapy, and immunotherapy. MedComm (2020). 2024; 5: e474.

Cite this article as: Gao T, Ito S, Moh-Moh-Aung A, Wang T, Fujisawa M, Ohara T, et al. SPRED2 suppresses the stemness of hepatocellular carcinoma through the p53/miR-506-3p/KLF4 pathway. Cancer Biol Med. 2026; x: xx-xx. doi: 10.20892/j.issn.2095-3941.2025.0247